Absolute Position Acquisition for Linear Synchronous Motor With Passive Mover

TUANSHAN ZHANG [1,2], **XUESONG MEI** [1], **AND XIN DU** [2]

[1]Department of Mechanical Engineering, Xi'an Jiaotong University, Xi'an, Shaanxi 710049, China
[2]Department of Mechanical and Electrical Engineering, Xi'an Polytechnic University, Xi'an, Shaanxi 710048, China

Corresponding author: Xuesong Mei (xsmei@mail.xjtu.edu.cn)

ABSTRACT The winding segmented permanent magnet linear synchronous motor has restrictions on the last absolute position acquisition when the power goes from off to on, and the traditional absolute position acquisition systems depend on complex battery and calibration systems. Therefore, a true absolute magnetic encoder based on the Vernier principle with error rejection and decoding technology is studied in this paper. First, the output signal of the magnetic encoder with noise was subjected to the adaptive ellipse parameter correction algorithm with recursive least squares (RLS), and the source output signal predicted and reconstructed. Furthermore, the RLS was optimized by the speed weighting factor and the forgetting factor to reduce the computational pressure and the iterative process. Second, one improved double second-order generalized integrator(DSOGI) decoding technology was investigated by extracting and separating the symmetric-positive sequence components in the unbalanced signal, and, using the phase-locked loop technique for tracking calculation, accurate speed and angle obtained. The adaptive ellipse parameter fitting algorithm effectively reduced the problem of overshoot and steady-state error of the DSOGI, which provides a practical and theoretical basis for the future application of the magnetic encoder. This trajectory arrangement not only avoids the influence of accumulated error on the accuracy of encoder, but it also solves the contradiction between high resolution and small volume, and the advantages over the special decoding chip IC-Haus were also verified by comprehensive experimental results.

INDEX TERMS Absolute magnetic encoder, Vernier decoding, ellipse parameter identification, recursive-least-squares dual second-order generalized integrator (RLS-DSOGI), winding segmented permanent magnet linear synchronous motor (WS-PMLSM).

I. INTRODUCTION

Linearelectrical motors are presently gaining increasingly widespread use in transportation [1] and industry (e.g., machining and actuators). Figure 1 shows an example for material handling and processing applications in which several vehicles (workpiece carriers) travel with a high degree of independence on the same track, four processing stations (P1-P4) are spread along the track, and the vehicles (V1-V4) move outside the processing stations [2].

To allow a high degree of independence in the movement of the vehicles, the stator (primary) of the linear machine is divided into many segments, where high-precision positioning is necessary for segment motors and mover

The associate editor coordinating the review of this manuscript and approving it for publication was Muhammad Imran Tariq [ID].
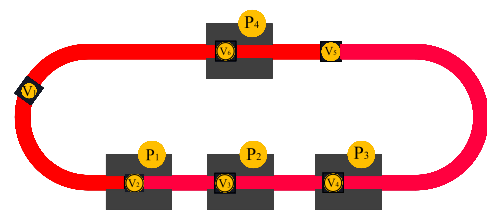

FIGURE 1. Simple example of proposed linear drive system.

vehicles. The standard solution for this application is based on a high-resolution optical encoder or a comparatively lower-resolution capacitive sensor [3]. For passive vehicles, passive scale must be attached to the vehicle, and the active reading head fixed and mounted along the track, as shown in Fig. 2. Each read head has a unique absolute length code

and an incremental bar grid structure. The method has the ability to measure the absolute position of several vehicles at the same time, including the measurement along, e.g., a curved track [4]. However, it is not easy to implement an absolute position sensing system in the case of power failure. Therefore, the prototype of absolute magnetic encoder based on Hall effect is studied in this paper, and the magnetic net adopted a unique double-track design based on Vernier decoding.
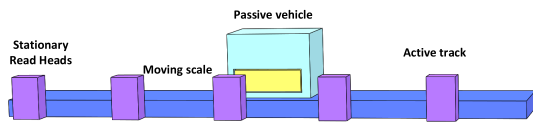

FIGURE 2. Position sensing using optical encoder.

Currently, the only microcircuit on the market for Vernier magnetic position sensors is a single-chip solution, namely, the IC-Haus microcircuit family, which integrates Hall elements, converters, and splice circuits, among other components, and it can be used in magnetic systems of different sizes [5]. Owing to its low thermal stability and susceptibility to interference from external magnetic fields, the output of the magnetic encoder will produce errors that cannot be suppressed by the dedicated IC-Haus decoder chip. Therefore, a software decoding technique was proposed to improve the decoding accuracy of the encoder.

At present, the most commonly used software decoding method is type II tracking phase-locked loop (PLL) technology [6]. It is widely used in the angle measurement systems of resolvers. Another common decoding method is the coordinate rotation digital computer (CORDIC [7]) used in decoder chip IC-Haus systems [8], which is an open-loop algorithm. However, this algorithm is easily affected by electromagnetic noise and other errors, and it exhibits poor anti-interference performance. Aiming at how to improve the calculation accuracy and error suppression ability of the decoding algorithm, a double synchronous reference-frame-based phase-locked loop (DSRF-PLL) method was proposed previously [9]. This method has high precision and can suppress the error signals, but its disadvantage is that it will increase the response time when decomposed to the double rotation coordinate system. Furthermore, the complex forward and reverse decoupling network and low-pass filter can increase the processing delay of the PLL [10], thereby affecting the transient response and stability of the closed-loop system.

The singular second-order generalized integral [11] has a good effect on fixed frequency, and to better suppress the error and improve decoding accuracy, in this paper a dual second-order generalized integrator (DSOGI) decoding technology is presented that can output orthogonal signals with equal amplitudes. Compared with the DSRF-PLL, this method has a simple structure and shorter response time. In light of the problem that the double generalized second-order integrator method has a poor effect on

the suppression of bias error, a recursive-least-squares dual second-order generalized integrator (RLS-DSOGI) decoding technology was presented, and the RLS-DSOGI decoding technology optimized to improve the calculation process of the algorithm. Although the ultra-least-squares fitting of circle and ellipse [12] is a high-precision ellipse fitting method, it is suitable for machine vision with strong computing power, and it is not very practical in the embedded system considered herein. The accuracy of the encoder was greatly improved after error compensation, which provides a theoretical basis for the future application of the decoder.

The rest of this paper is organized as follows. In Section II, the overall design of a Hall-type magnetic encoder and spatial magnetic field distribution of the magnetic gate of the magnetic encoder are presented. The error compensation algorithm of the magnetic encoder is provided in Section III. In Section IV, comprehensive experimental results are presented. Finally, conclusions are drawn in Section V.

II. OVERALL DESIGN OF HALL-TYPE VERNIER MAGNETIC ENCODER

A. MAGNETIC GRID STRUCTURE

A conventional absolute grating ruler obtains absolute position information by reading the position code [13]. The scale grating is shown in Fig. 3, which is characterized by periodic grating scribes and an encoding that includes absolute position information. Each time the machine is turned on, the absolute raster ruler depicted in the figure can obtain the absolute position information by reading the current position code, but the accuracy is low.
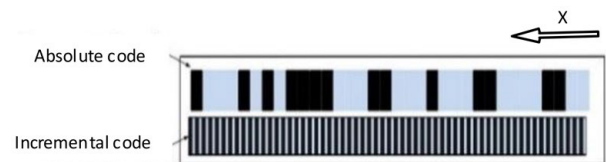

FIGURE 3. Traditional absolute grating ruler.

In this paper, a magnetic system in which the incremental gate is made according to the Vernier principle to achieve the absolute characteristics of data is studied. The gate is stitched out from a two-scale system with a specific proportion of scale periods [14]. The key nodes of the system are a sensor system and processing circuit. The sensor system can be implemented using external magnetoresistance and Hall elements. As the basic component of a magnetic encoder, the magnetic gate directly determines the overall performance of a magnetic encoder. The accuracy of absolute magnetic gate scales consists of two parts: the position accuracy of the whole length and the subdivision accuracy of the moire fringes in the signal cycle. Therefore, in this application, a high-precision, single-channel, absolute-position-coding, absolute-grating-ruler (Fig. 3) is unrealistic. Figure 4 shows the magnetic gate based on the Vernier principle in this design, which is reproduced from [15].
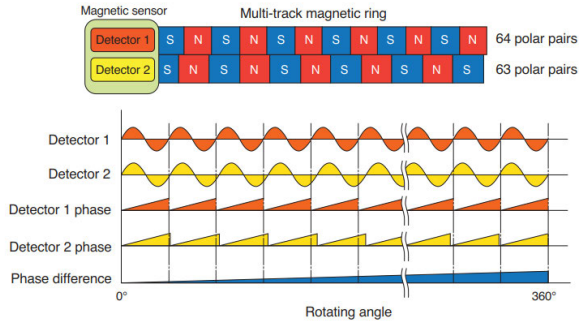
FIGURE 4. Magnetic gate based on Vernier principle.

The principle of Vernier measurement was first proposed by the French mathematician Pierce Vernier. The Vernier caliper is the most classic application of this principle [16]. The conceptual principle of the Vernier cursor is to use two sets of periodic data separated by one period difference in the same range to determine the absolute position measurement. Therefore, in the design of a magnetic encoder, the absolute position information must be calculated, and the initial data need two groups of analog signals that differ by one cycle. It is assumed that the original signals output by the magnetic sensing element are two sets of sinusoidal signals, namely, signals A and B. The magnetic gate has two analog signals in one period, with the number of cycles being 64 and 63, respectively, as shown in Fig. 5.
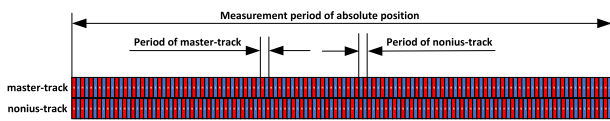

FIGURE 5. Schematic of Vernier solution.

The actual angles of two groups of signals can be expressed as follows:

$$\theta_A = \frac{360°}{n} \times m_A + p_A \tag{1}$$

$$\theta_B = \frac{360°}{n-1} \times m_B + p_B \tag{2}$$

where θ_A and θ_B are the actual angles corresponding to signals A and B, respectively, n is the reference period number of signals in one cycle (in this case, n = 64), m_A and m_B are the complete cycles of signals A and B, respectively, and p_A and p_B are the angles corresponding to the incomplete cycles of signals A and B, respectively.

Considering $\theta_A = \theta_B$, the difference between the two formulas is

$$p_A - p_B = \frac{360°}{n-1} \times m_B - \frac{360°}{n} \times m_A \tag{3}$$

Because signal A has one more cycle than signal B over one mechanical cycle, there are two cases for the relationship between m_A and m_B when going through the same mechanical angle:

1. When $m_A = m_B = m$,

$$p_A - p_B = \left(\frac{360}{63} - \frac{360}{64} \right) \times m = \frac{5}{56} \times m \tag{4}$$

2. When $m_A = m_B + 1 = m$,

$$p_A - p_B = \left(\frac{360}{63} - \frac{360}{64} \right) \times m - \frac{40}{7} = \frac{5}{56} \times m - \frac{40}{7} \tag{5}$$

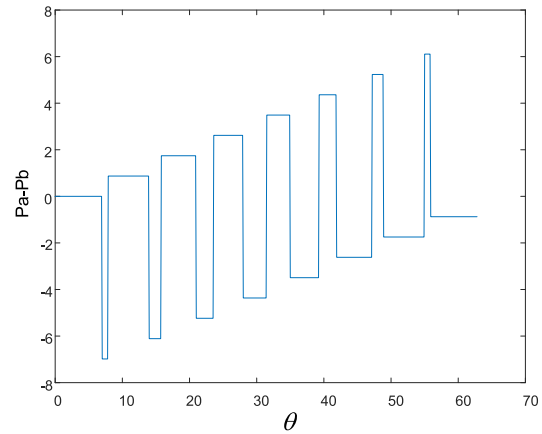The plot of p_A-p_B versus θ [created in MatLab (Math-Works, USA)] is shown in Fig. 6.

FIGURE 6. Relationship between p_A-p_B and θ.

From the figure, if one elimnates the negative, one obtains the value m, and m is replotted in Fig. 7.
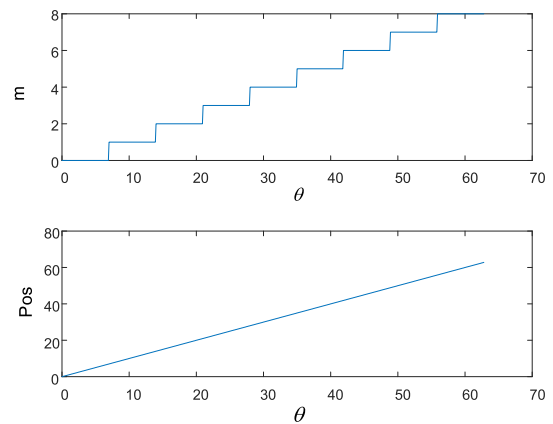

FIGURE 7. Relationship between m, pos, and θ.

The value of p_A-p_B has different values at different mechanical angles. Depending on the characteristics of the initial signal, there are only two relationships between m_A and m_B for any number of cycles. Thus, the value of m can be found by directly calculating the value from p_A-p_B and θ, and the mechanical angle can be obtained as follows:

$$\theta_A = \frac{360°}{64} \times m + P_A \tag{6}$$

Figure 7 shows the angle position information corresponding to the length, and the process of absolute position acquisition is shown to be linear; the current goal is to solve this kind of problem.

B. ABSOLUTE POSITION PROCESS

Based on the discussion above, to obtain the angle position, the signal-generating component must provide two groups of original signals with one electric cycle difference. Therefore, the form of a parallel double-code-track magnetic gate and a double Hall element were used in this work to satisfy this algorithm. In addition, considering the actual design requirements, such as the size of the magnetic gate and the arrangement of the double-code pole positions, the cycle number of the designed upper and lower code channels was determined to be 64 and 63, respectively. The total length was 174 mm, absolute measurement range 163.84 mm, and carrier material was steel 1.4310K2. Figure 8 shows the physical figure.
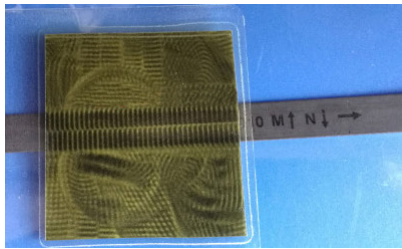

FIGURE 8. Two-track Nonius magnetic tape.

In this work, a TMR2102 chip was selected as the Hall signal processing chip, which used a unique push-pull Wheatstone full-bridge structure design, including four un-shielded high-sensitivity TMR sensor elements. When the sensitive direction changed, the entire Wheatstone bridge provided a differential voltage output, and one read head was needed for four TMR2102 chips. The block diagram of the processing unit is shown in Fig. 9. The sensor operated as follows. Magnetic tape was mounted on a passive mover, and sensors (1) and (2), corresponding to the master track, produced sine/cosine differential signals (SINP1, SINN1, COSP1, and COSN1). Sensors (3) and (4), corresponding to a Nonius track, produced sine/cosine differential signals (SINP2, SINN2, COSP2, and COSN2). The differential signals from the read heads were analog sine and cosine signals, for which filtering and analog-to-digital conversion, ellipse recognition, and correction could be processed by the recursive-least-squares dual-second-order generalized integrator (RLS-DSOGI) decoding technology. Thus, the sine/cosine signals of the sensor systems were converted into digital phase codes φ_m and φ_n of the master and Vernier tracks.

Here, φ_m and φ_n were equal to p_A and p_B, respectively. The absolute position was then calculated according to the above formula.
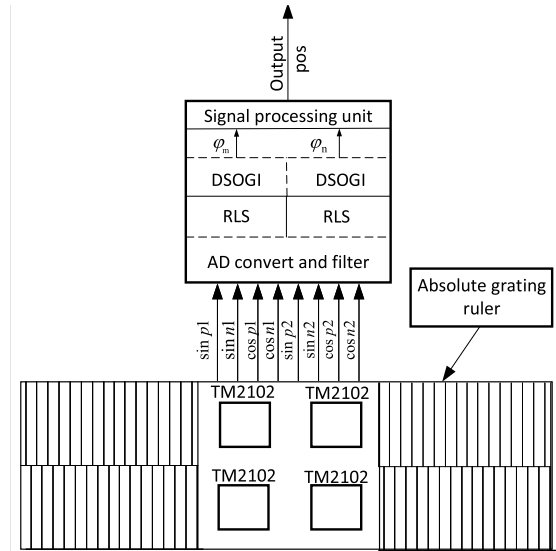

FIGURE 9. Read-head process block diagram.

C. ABSOLUTE POSITION ACQUISITION

While the processing circuit of each reader was described above, how to obtain the linear distance of a passive mover must still be determined. In the case of a passive mover, the length of the sensor's scale is limited to the length of the mover. If a travelling distance longer than the mobile component is required, more than one read head will be necessary. In the proposed system, four read heads were spread along the carriageway separated from each other by approximately 125 mm. Thus, the 163-mm-long scale covered at least one read head at any given position. Because it was not feasible to mount the heads at distances with higher repeatability than ± 0.01 *mm*, it was necessary to calculate and compensate for the difference between the phases of two neighboring heads (as determined by the arctangent function). When the scale passed from one read head to the next, the signals from both heads would be simultaneously evaluated once, and the initial position of the incoming read head could be calculated. Future position calculations were based on this initial value. Thus, a monotone variation of the calculated position along the entire measuring length could be ensured as shown in Fig. 10, which is reproduced from [3].
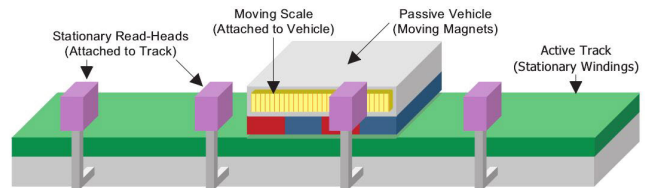

FIGURE 10. Position sensing with magnetic encoder.

The circuit timing logic processing of the four read heads is relatively complicated, which is not the focus of this discussion, but it will be discussed in a planned future article.

This circuit selects a Xilinx XC6LX16 chip as the signal processing circuit; the chip adopts the CPG196 package. It has the advantages of small size, many internal logic units, and strong processing ability, which is beneficial to the design of integrated circuits.

III. ERROR ANALYSIS AND IDENTIFICATION OF ELLIPSE PARAMETERS

A. ERROR ANALYSIS

In the magnetic encoder, the magnetic gate and Hall element constitute the signal-generating component. In an ideal scenario, the magnetic gate designed in the present work would be installed in parallel with the Hall chip, and the Hall chip would be aligned with the center line of the magnetic pole on the magnetic gate code track. However, in an actual manufacturing and installation process, various errors will inevitably occur [17]. This can be seen from the waveform of the magnetic encoder, as shown in Fig. 11, the sinusoidal form has been seriously affected, which cause some errors in the output voltage, according to the different forms of errors, these errors are divided into bias error, amplitude error, phase error, harmonic error.
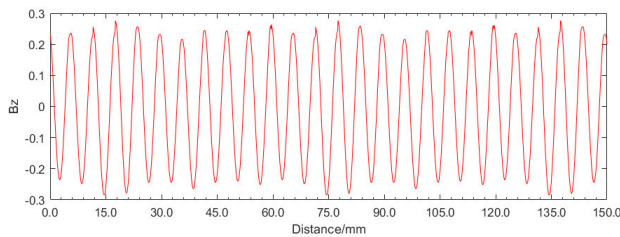

FIGURE 11. Waveform of magnetic encoder.

The presence of these errors may affect the output signal and overall performance of the encoder. Therefore, it is necessary to analyze the factors that may affect the error and determine how to compensate for the error. The error sources of a magnetic encoder signal during manufacturing and installation mainly include amplitude, phase, bias, and harmonic errors. To prevent these errors, it is necessary to optimize the decoding method and improve the anti-jamming ability of the decoding algorithm; meanwhile, it is necessary to limit all kinds of errors in a certain range when designing the encoder prototype.

B. ERROR COMPENSATION

Theoretical derivations show that when using type II tracking PLL decoding [18] the existence of amplitude and phase errors cause the oscillation frequency between the decoding and real angles to double the mover speed, and the presence of bias error causes the calculation result to produce an oscillation frequency equal to the mover speed. Therefore, it is necessary to study a new decoding technology that can suppress the error and improve the accuracy of the decoding system.

As shown in the literature, when the mover speed is fixed, the dual generalized second-order integrator decoding algorithm can effectively eliminate the amplitude and phase errors of the magnetic encoder signal. However, in practice, the signal of the magnetic encoder exhibits some DC bias error [19], while the mover speed is not fixed. Through simulations and experiments of the DSOGI decoding technology, it was found that the performance of the decoding algorithm of the DSOGI requires further improvement [20].

The original DSOGI algorithm cannot accurately calculate the speed and angle information [21], so a RLS-DSOGI decoding technology is proposed here. The entire decoding process consists of two parts: First, the parameters of the magnetic encoder are identified and corrected through the parameter identification link based on ellipse fitting technology [22], after which the improved DSOGI is used to calculate accurate angle and speed information.

C. IDENTIFICATION OF ELLIPSE PARAMETERS

Assuming that there are three common errors, i.e., amplitude, phase, and bias errors [23], the signal of the encoder is expressed as follows:

$$\begin{cases} U_s = A_1 \sin\theta + B_1 \\ U_c = A_2 \cos(\theta + \phi) + B_2 \\ U_{ns} = A_3 \sin\theta_1 + B_3 \\ U_{nc} = A_4 \cos(\theta_1 + \phi_1) + B_4 \end{cases} \quad (7)$$

In these equations, U_s and U_c are outputs of the master track, and U_{ns} and U_{nc} are outputs of the Nonius track. Here, the master track is taken as an example, and the same applies to the Nonius track. A_1 and A_2 are the amplitude of the sine and cosine signals of the master track, respectively; B_1 and B_2 are the offset components of the sine and cosine of the master track, respectively; and ϕ is the phase error. A_1, A_2, B_1, B_2, and ϕ are the parameters of the magnetic encoder. When these signals are decomposed into orthogonal planes, the trajectory is an ellipse, and A_1, A_2, B_1, B_2, and ϕ become parameters of the elliptic equation. After the ellipse parameters are obtained, the position information can be obtained by the following formula:

$$\begin{cases} \sin\theta = \dfrac{U_s - B_1}{A_1} \\ \cos\theta = \dfrac{\frac{U_c - B_2}{A_2} + \sin\phi \sin\theta}{\cos\phi} \end{cases} \quad (8)$$

Using elliptical parameters to reconstruct the actual output signal of magnetic encoder with errors, the magnetic encoded signal is changed from an ellipse to ideal circle, and the subsequent DSOGI calculations are greatly reduced.

Among the existing ellipse fitting algorithms, such as the fitting algorithms applied to pattern and image recognition, most are used for offline fitting of data samples or require strong computing power. Therefore, these methods are difficult to be used in real-time systems with limited computing power and memory. The least-squares technique is mainly

used to find a set of parameters to minimize the measurement of the distance between the data points and the ellipse. The common distance measures include geometric and algebraic distance. However, the expression of the objective function of the geometric fitting method is very complex, so the solving process is very heavy and difficult to realize. Therefore, this paper improves the algebraic fitting method, aiming at solving the problem that the contribution of each parameter is different in the algebraic fitting.

Fitzgibbon proposed an effective method of ellipse fitting for discrete data based on a direct least-squares method [8]. However, due to the complexity of the calculation and poor real-time performance, it is difficult to directly apply this for the adaptive technology and calibration of the signal parameters of a magnetic encoder with high real-time requirements. Therefore, it is necessary to further optimize this algorithm, simplify the calculation process, and improve the real-time performance. Combining the equations in Eq. (8) and eliminating ϕ yields the following:

$$\left(\frac{U_c - B_2}{A_2 \cos \phi}\right)^2 + \left(\frac{U_s - B_1}{A_1 \cos \phi}\right)^2 \sin^2 \phi + \frac{2 \sin \phi}{A_1 A_2 \cos^2 \phi} \\ (U_c - B_2)(U_s - B_1) = 1 \quad (9)$$

which can be written as

$$U_c^2 = \alpha_1 U_s^2 + \alpha_2 U_s U_c + \alpha_3 U_s + \alpha_4 U_c + \alpha_5 \quad (10)$$

where α_1, α_2, α_3, α_4, and α_5 are the regression parameters. The constraints are subject to the following elliptic equation constraints:

$$\alpha_1 < 0, \alpha_2 < 0, 4\alpha_1 + \alpha_2^2 < 0 \quad (11)$$

By comparing the regression parameters in Eq. (9) with the corresponding coefficients in Eq. (10), the ellipse signal parameters of the magnetic encoder can be determined using the regression parameters. The parameters are as follows:

$$\begin{cases} \phi = \arcsin\left(\frac{-\alpha_2}{2\sqrt{-\alpha_1}}\right) \\ B_1 = -\frac{2\alpha_3 + \alpha_2\alpha_4}{4\alpha_1 + \alpha_2^2} \\ B_2 = \frac{2\alpha_1\alpha_4 - \alpha_2\alpha_3}{4\alpha_1 + \alpha_2^2} \\ A_2 = \frac{\sqrt{\alpha_5 + B_2^2 + 2B_1 B_2 \sin \phi \sqrt{-\alpha_1} - \alpha_1 B_1^2}}{|\cos \phi|} \\ A_1 = \frac{A_2}{\sqrt{-\alpha_1}} \end{cases} \quad (12)$$

When using the recursive-least-squares (RLS) method to correct the signal parameters of the magnetic encoder, each iteration should minimize the following error functions:

$$E(n) = \sum_{i=1}^{n}\left\{\lambda^{n-i}\left(y(i) - \underline{a}(n)^T \cdot \underline{x}(i)\right)^2\right\} \quad (13)$$

where $\underline{\alpha}(n) = \left[\alpha_1(n), \underline{\alpha}_2(n), \underline{\alpha}_3(n), \underline{\alpha}_4(n), \underline{\alpha}_5(n)\right]^T$, $\underline{x}(i) = \left[U_{\sin}(i)^2, U_{\sin}(i)U_{\cos}(i), U_{\sin}(i), U_{\cos}(i), 1\right]$, $y(i) = U_{\cos}(i)^2$

α_n is the regression parameter when iterating n times, $\lambda^{(n-i)}$ the forgetting factor, and $y(i)$ the regression output. During operation, the problem of frequent acceleration and deceleration of the motor will be encountered, resulting in an uneven distribution of data points around the ellipse. If the original least-squares method is directly used for ellipse fitting, these densely distributed data points will take up too many computing resources, resulting in overfitting problems and distortion of the parameter discrimination. Therefore, the original algorithm should be further optimized, and no matter what the spatial distribution density of data points is, all of the data points can participate in the fitting process uniformly and avoid false fitting. Supposing that $N(t)$ is the number of data points sampled at time t, the RLS error function must be optimized so that the impact of each data point is proportional to the reciprocal of the spatial density of the data.

$(dN/dt)^{(-1)}$ is the sampling rate and is a constant, so the error function given by Eq. (13) can be simplified and written as follows:

$$E'(n) = \sum_{i=1}^{n}\left\{\lambda^{n-i}\left|\frac{dN}{d\theta}\right|^{-1}\left(y(i) - \underline{\alpha}(n)^T \underline{x}(i)\right)^2\right\} \quad (14)$$

where $\left(\frac{dN}{d\theta}\right)^{-1} = \left(\frac{dN}{dt}\right)^{-1}\frac{d\theta}{dt}$

$(d\theta/dt)$ is the angular velocity and $(dN/dt)^{(-1)}$ is a constant, so the error function given by Eq. (14) can be simplified and written as follows:

$$E'(n) = \sum_{i=1}^{n}\lambda^{n-i}\left\{|w(i)|\left(y(i) - \underline{\alpha}(n)^T \underline{x}(i)\right)^2\right\} \quad (15)$$

where the $w(i)$ is the mover velocity (linear displacement) calculated by the axis angle tracking (including the sampling time constant). To avoid errors of the RLS method and reduce the number of computations, the position of the mover is introduced into the algorithm. In the forgetting factor $\lambda^{(n-i)}$, the exponent$(n - i)$ represents the time interval in time $[i, n]$, which is replaced by the linear displacement of the mover in time $[i, n]$. Thus, the original iterative algorithm with time updating is improved to an iterative calculation with the mover displacement updating, which reduces the number of computations required of the algorithm and optimizes the iterative process. The angle function is expressed as follows:

$$g(i, n) = \begin{cases} \sum_{j=i+1}^{n}|\theta(j) - \theta(j - 1)|, & i < n \\ 0, & i \geq n \end{cases} \quad (16)$$

where θ is the angle (corresponding to the linear displacement) calculated by the DSOGI. Introducing the angle function $g(i, n)$, the error function can be rewritten as follows:

$$E''(n) = \sum_{i=1}^{n}\left(y'(i) - \underline{\alpha}(n)^T \underline{x}'(i)\right)^2 \quad (17)$$

where $y'(i)$ and $x'(i)$ are auxiliary variables:

$$\begin{cases} \underline{x}'(i) = \lambda^{g(i,n)'/2}|w(i)|^{1/2}\underline{x}(i) \\ \underline{y}'(i) = \lambda^{g(i,n)'/2}|w(i)|^{1/2}\underline{y}(i) \end{cases} \quad (18)$$

The parameters $\alpha(n)$ of the error function given by Eq. (17) are the least-squares solutions given by the following equation:

$$\underline{\alpha}(n) = [\phi(n)]^{-1}\underline{\psi}(n) \quad (19)$$

In Eq. (19),

$$\begin{cases} \phi(n) = \sum_{i=1}^{n}\left\{\lambda^{g(i,n)}|\omega(i)|\left(\underline{x}(i)\underline{x}(i)^{T}\right)\right\} \\ \underline{\psi}(n) = \sum_{i=1}^{n}\left\{\lambda^{g(i,n)}|\omega(i)|\left(\underline{x}(i)y(i)^{T}\right)\right\} \end{cases} \quad (20)$$

It is more complex to solve Eq. (16) directly, and the computational complexity increases with time, making solving difficult. The recursive form of the iterative parameters $\underline{\alpha}(n)$ must be further derived. Using Eq. (16), one obtains

$$g(i, n) = g(i, n - 1) + |\theta(n) - \theta(n - 1)| \quad (21)$$

The iteration formulas of $\phi(n)$ and $\psi(n)$ are as follows:

$$\phi(n) = \lambda^{|\theta(n)-\theta(n-1)|}\phi(n-1) + |\omega(n)|\underline{x}(n)\underline{x}(n)^{T},$$
$$\underline{\psi}(n) = \lambda^{|\theta(n)-\theta(n-1)|}\underline{\psi}(n-1) + |\omega(n)|\underline{x}(n)y(n)$$

The RLS method adopts the matrix algorithm to obtain the following recursive formula:

$$\phi^{-1}(n) = p(n) = \frac{p(n-1) - \underline{k}(n)\underline{x}(n)^{T}p(n-1)|\omega(n)|^{1/2}}{\lambda^{|\theta(n)-\theta(n-1)|}} \quad (22)$$

where $\underline{k}(n) = \frac{|\omega(n)^{1/2}p(n-1)x(n)|}{\lambda^{|\theta(n)-\theta(n-1)|}+|\omega(n)|\underline{x}(n)^{T}p(n-1)\underline{x}(n)}$.

By combining the formulas above, the recursive form of the parameter $\alpha(n)$ is obtained:

$$\underline{\alpha}(n) = \underline{\alpha}(n - 1) + \underline{k}(n)e(n) \quad (23)$$

where $e(n) = |\omega(n)|^{1/2}\left(y(n) - \underline{\alpha}(n-1)^{T}\underline{x}(n)\right)$.

The above theoretical calculation shows that RLS-DSOGI decoding technology can effectively suppress the amplitude, phase, and bias errors in the output signal of the magnetic encoder. The algorithm was optimized for specific problems to further improve the decoding accuracy and reduce the computational pressure.

D. MODELING SIMULATION ANALYSIS

Figure 12 is a block diagram of the RLS-DSOGI decoding technology, including parameter identification and correction, as well as velocity and angle calculation. This block diagram is derived from Eq. (8).

U_c and U_s are the voltage signals of the main channel or Vernier channel processed by simple filtering, as mentioned before, which contain a variety of error signals; V_α and V_β
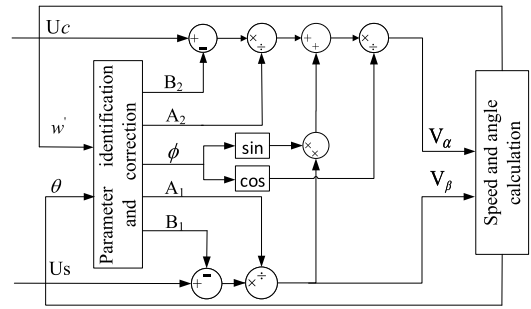

FIGURE 12. Block diagram of RLS-DSOGI.

are standard circular signals. Simulink was used to build a simulation verification platform to verify the improved error suppression decoding algorithm. The effectiveness of the method is verified by changing the amplitude, phase, offset, and harmonic of the input signal. Therefore, before parameter identification, the input signal contains the aforementioned four kinds of errors, as shown in Fig. 13.
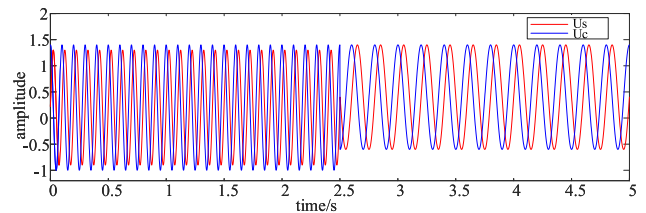

FIGURE 13. Input signal waveform.

The input signal is, when $t \leq 2.5$s,

$$\begin{cases} U_s = 1.1\sin(20\pi t + \pi/180) + 0.2 \\ U_c = 1.2\cos(20\pi t) + 0.2 \end{cases} \quad (24)$$

and, when $t > 2.5$s,

$$\begin{cases} U_s = \sin(10\pi t) + 0.4 \\ U_c = \cos(10\pi t) + 0.4 \end{cases} \quad (25)$$

The output waveform of the input signal containing errors after parameter identification and correction is shown in Fig. 14. After 2.5 s, the ellipse fitting based on RLS reconstructed the two-phase non-ideal signal containing errors into an ideal signal with the same amplitude and orthogonal phase, which shows the effectiveness of parameter identification and correction.
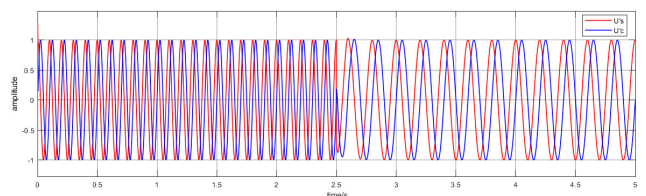

FIGURE 14. Signal corrected by ellipse fitting.

E. RLS-DSOGI SIMULATION ANALYSIS

After applying the adaptive parameter identification algorithm, the output signal V_α and V_β signal are contained in the high-frequency harmonic and mixed with the untreated clean error signal. To follow up on the decoding accuracy, the improved DSOGI is adopted. The DSOGI, based on the principle of intima, has been applied in power systems. In this paper, it is used to realize the orthogonal transformation of signals to obtain the positive sequence components of the two confidence signs of the encoder. Its principle is shown in Fig. 15.
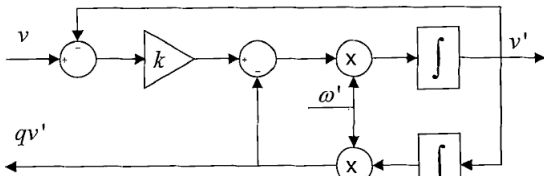
FIGURE 15. Generalized second-order integrator diagram.

The transfer function of the system is

$$\begin{cases} D(s) = \dfrac{v'(s)}{v(s)} = \dfrac{kw's}{s^2 + kws + w'^2} \\ Q(s) = \dfrac{qv'(s)}{v(s)} = \dfrac{kw'^2}{s^2 + kws + w'^2} \end{cases} \quad (26)$$

where w' is the resonance frequency of the system, w the input signal frequency, and k the generalized second-order integrator control parameter.

By intensively analyzing the existing work, the second-order generalized integrator (SOGI) has been commonly used for filtering, quadrature signal generation, and phase traction. The SOGI can be considered as a filter combined with an integrator. Moreover, the amplitude attenuation and phase shift can be avoided. The theoretical calculation shows that this new type of decoding scheme can restrain the error of the encoder signal adaptively, and the existing amplitude and phase errors can be extracted by SOGI separation.

In [24], two different discretization ideas are put forward and experimental verification conducted. In [25], forward Euler, backward Euler, bilinear discretization, and other methods are compared, and it is found that forward and backward Euler methods would make the output signal lose its orthogonality. To ensure the orthogonality of the output signal, the bilinear method is used to discretize DSOGI. The common second-order generalized integrator based on Euler difference can realize the orthogonal coordinate transformation through $T_s/(1 - z^{-1})$ to approximate $1/s$ to achieve system discretization. Generalized second-order integrals are implemented by a third-order integral through $T_s(23z^{-1} - 16z^{-2} + 5z^{-3})/k(1 - z^{-1})$ to approximate $1/s$, and the discretized third-order integral can be expressed as follows:

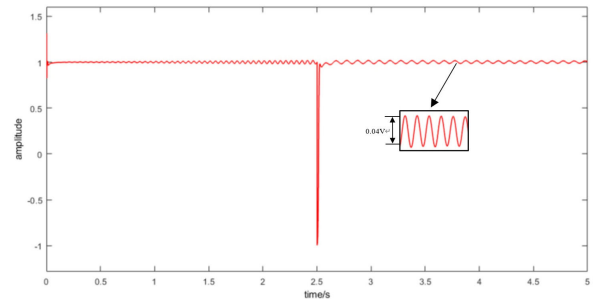$$y(n) = y(n-1) + \frac{T}{k}[23u(n-1) - 16u(n-2) + 5u(n-3)] \quad (27)$$
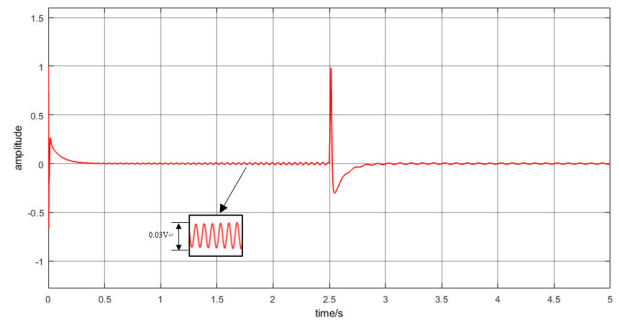

FIGURE 16. Vq by DSOGI without RLS.

FIGURE 17. Vd by DSOGI without RLS.

Simulation verification was carried out under two different conditions. V_d represents the phase tracking characteristics, V_q the speed tracking characteristics, w the speed output, and theta(θ) the position output.

The first case is the step response of V_q and V_d, and the input signal is halved at 2.5 s, which is shown in Fig. 13. The output waveforms of V_q and V_d without parameter identification are shown in Figs. 16 and 17, respectively. The output waveforms of V_q and V_d with parameter identification are shown in Figs. 18 and 19, respectively.
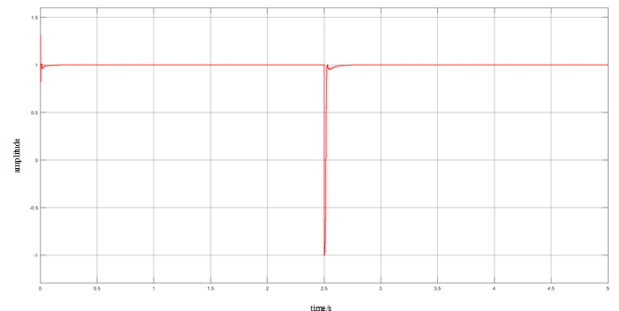

FIGURE 18. Vq by DSOGI with RLS.

As can be seen from the figure, the fluctuation of V_q with RLS in the steady state is zero; however, a fluctuation of 0.05 appears in the system without RLS. The dynamic performance is basically the same. The difference in phase tracking characteristics is quite obvious, and the fluctuation of V_d without RLS parameter identification in the steady and dynamic states is larger than that with RLS.
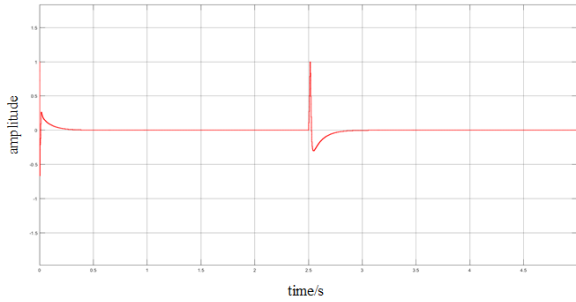
FIGURE 19. Vd by DSOGI with RLS.

The second case is the angular waveform output after parameter identification and correction of the input signal containing errors when the motor speed changes as shown in Fig. 13. The calculated angular displacement of RLS-DSOGI decoding technology is shown in Fig. 20. When the angular velocity is halved, the angular displacement changes are quickly identified. What is finally desired is the absolute position. From the simulation results, there is no deviation in the position, which meets the design requirements.
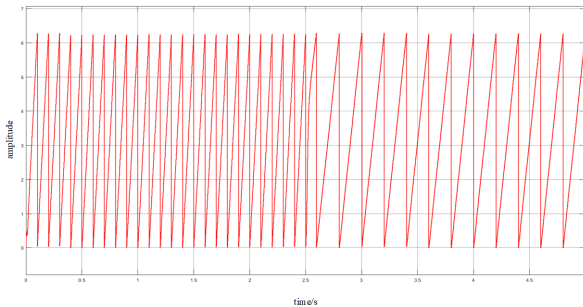

FIGURE 20. RLS-DSOGI calculated angular displacement.

The third step is the transient performance of the test algorithm when the motor speed changes. The input signal is, when $t \leq 2$s,

$$\begin{cases} U_s = 1.1\sin(40\pi t + \pi/180) + 0.2 \\ U_c = 1.1\cos(40\pi t) + 0.2 \end{cases} \quad (28)$$

and, when $4 > t > 2$s,

$$\begin{cases} U_s = \sin((40\pi + 20\pi t)t) + 0.25 \\ U_c = \cos((40\pi + 20\pi t)t) + 0.3 \end{cases} \quad (29)$$

and, when $t \leq 6$s,

$$\begin{cases} U_s = 1.1\sin(120\pi t) + 0.25 \\ U_c = \cos(120\pi t) + 0.25 \end{cases} \quad (30)$$

The input signal containing error parameter identification and correction is shown in Fig. 21. The frequency changes from 2 to 4 s and contains errors of the input signal waveform that can be changed to the ideal signal with the same amplitude and orthogonal phase.
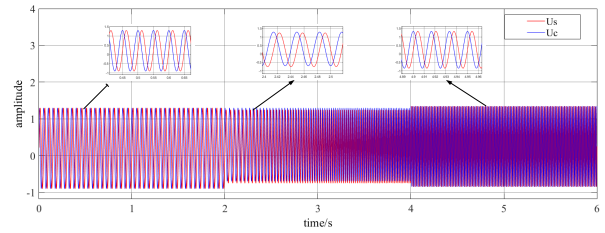
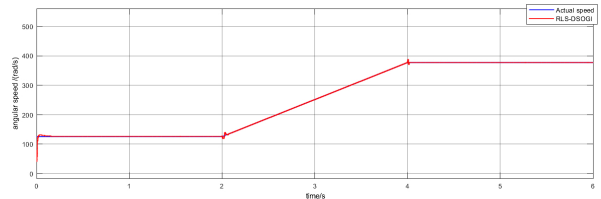FIGURE 21. Input signal waveform.

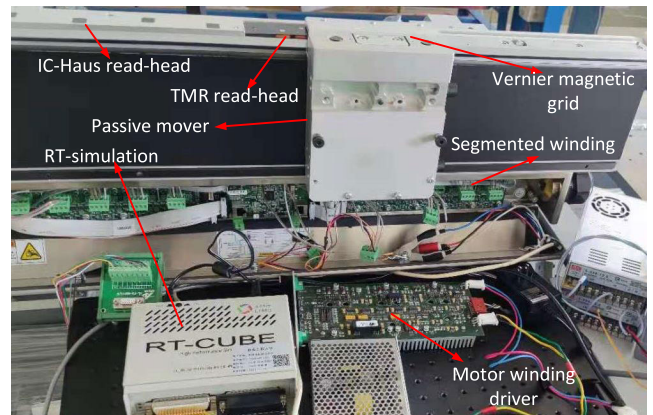FIGURE 22. RLS-DSOGI calculated speed and actual speed.

FIGURE 23. Experimental platform.

The calculated speed waveform of RLS-DSOGI decoding technology is shown in Fig. 22. The RLS-DSOGI decoding technology can fully suppress errors when the motor speed changes, and it exhibits a good dynamic response, which can track the frequency change of the input signal relatively stable and quickly with little fluctuation.

IV. EXPERIMENTAL RESULTS

In addition to the simulations, RLS-DSOGI decoding technologies were tested, and the decoding results were compared with the IC-Haus decoding results to further study the decoding accuracy and transient performance of the RLS-DSOGI decoding technology. This experiment was not combined with motor control in closed-loop control operation, but only the absolute position detection was studied.

The RLS-DSOGI and other decoding algorithm were completed in a RT-MATLAB environment constructed by the semi-physical real-time system provided by LinksRT (Beijing LINKS Technology Co., Ltd., Beijing, China), including an A/D board (Ni6259) for analog input and a D/A board (Ni6216) for digital output for encoder signal
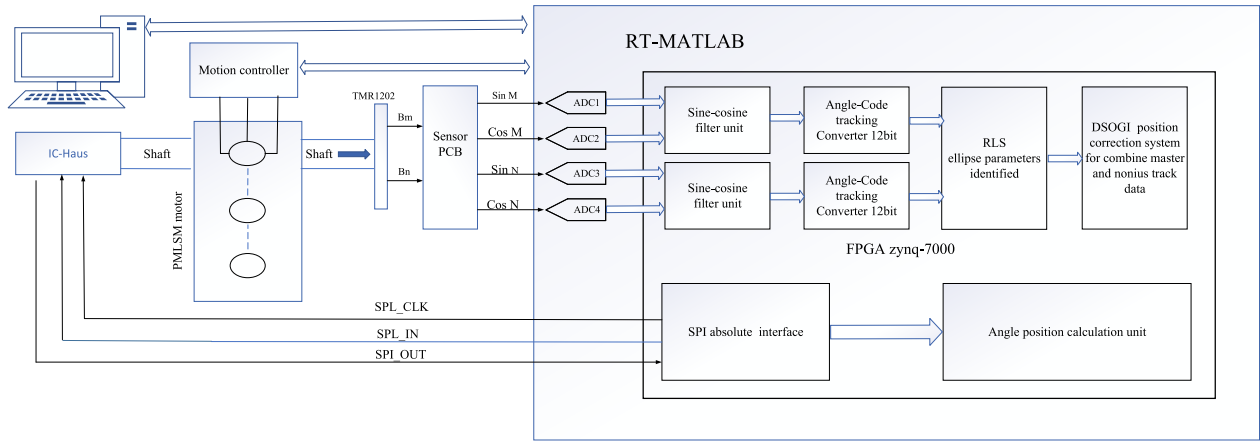
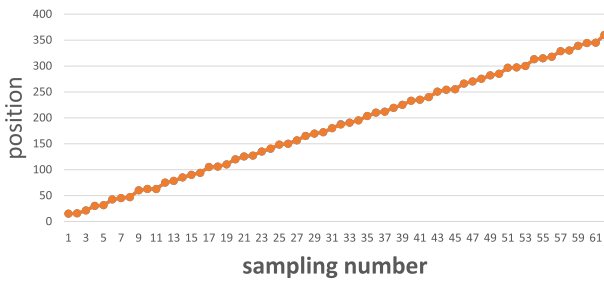**FIGURE 24.** Principle block diagram of experimental platform.

FIGURE 25. Position waveforms.

FIGURE 26. Position error waveforms.

simulation. The core components are of the Xilinx ZYNQ 7000 series. The Zynq-7000 SoC family integrates the software programmability of an ARM processor with the hardware programmability of an FPGA for critical analysis and hardware acceleration, while highly integrating CPU, DSP, ASSP, and mixed-signal functions on a single device. The Zynq-7000 family is a fully scalable SoC platform with the highest cost performance per unit power, which can fully meet unique application needs and be ported to our actual systems (xc6lx16).The IC-Haus system was purchased from Bosch, and Fig. 23 shows the physical drawing of the inspection platform.

The principle block diagram of the experimental system is shown in Fig. 24. The experiment was carried out in three steps.

The first step was to completely simulate the true operation of a linear motor; the sensor is driven back and forth by a linear guide, and the output voltage of the magnetic encoder was tested in a laboratory environment using a virtual instrument system, as shown in Fig. 25. The figure shows the results of operation of the model: by linking the outputs of master track and Nonius track convertors, and the phase difference data, the absolute position encoding between them is obtained. Experimental results are in good agreement with the theoretical analysis requirements. For the purposes of the present study, to obtain the absolute position, the figure above verifies the correctness of the decoding of the Vernier encoder, and Fig. XXXX verifies the accuracy of the position.
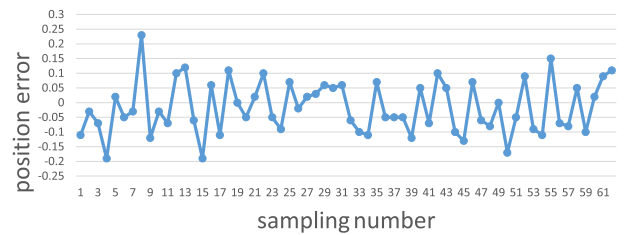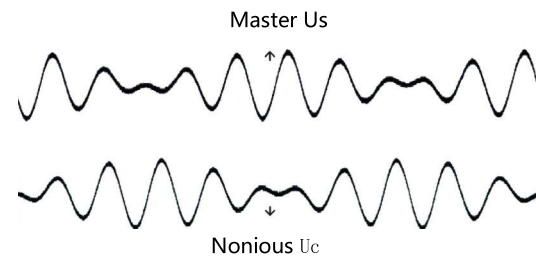

FIGURE 27. Simulation waveforms of TMR read head.

As can be seen from Fig. 26, among the 63 different calibration points, the IC-Haus's position error curve is highly nonlinear, and the maximum accuracy error reaches 0.23p>(13.8'). After analysis, the error of the encoder's output data is mainly due to the random error caused by the magnet performance, magnetizing process, and assembly error.

The second step is to compare static error indicators between the IC-Haus and RLS-DSOGI. Since the sensor error is a random signal, to observe the influence of various errors on the system at any time, RT-Cube is used to simulate various error information, so that the system performance can be obtained at any time. The measured signal of the magnetic encoder is shown in Fig. 27, which shows that it is not a standard sinusoidal signal.

In the experiment, the position error comparison between the IC-Haus special decoding chip and the RLS-DSOGI decoding algorithm is shown in Fig. 28.
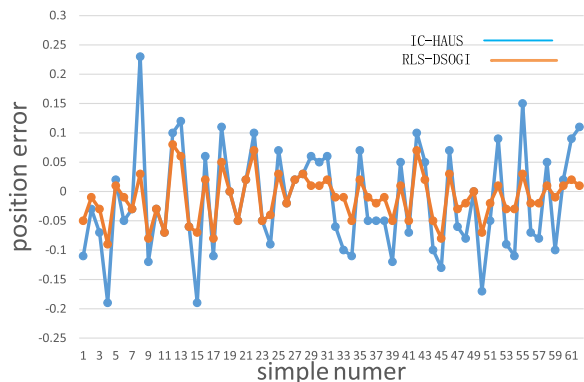
FIGURE 28. Error comparison between IC-Haus and RTS-DSOGI.

Experimental results show that even if the error ratio was very small, it still had a great impact on the position calculation results. After comparison, it was found that the RLS-DOSGI decoding technology could track the change of the mover position accurately and stably with little fluctuation.

In the third step, to verify the dynamic performance, the virtual linear motor was used to simulate the output voltage of the magnetic encoder in the laboratory environment by using the virtual instrument system. In this way, the dynamic performance data are easier to obtain. In the experiment, error signal is added to the output of the encoder, the amplitude error is 1%, and the phase error is 1. It was assumed that the motor speed remained unchanged at 5 Hz to obtain the angle measurement waveform at the same speed, which is convenient for comparison. The angle calculation results of each method are shown in Fig. 29.
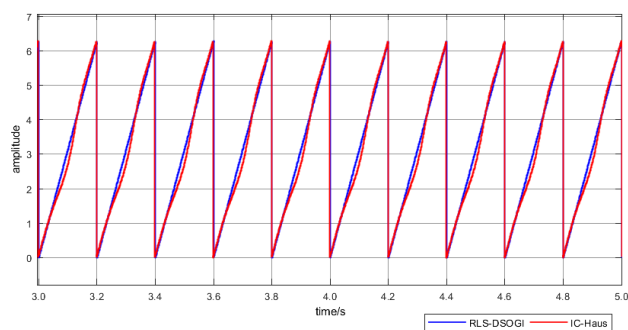

FIGURE 29. Speed calculated by RLS-DSOGI.

Figure 29 shows that the angle waveform measured by the RLS-DSOGI decoding technology was relatively smooth and fluctuated less, which was closer to the actual result.

The above experimental results showed that RLS-DSOGI exhibited an error suppression effect. This new decoding technology could adaptively suppress and correct the output error of the encoder. Compared with the existing SRF-PLL and special chip decoding technology, RLS-DSOGI has the advantages of good transient response and small steady-state error, and of a bad environment caused by the output error

of the encoder. A good restraining effect can improve the measurement accuracy of the motor speed and angle.

V. CONCLUSION

For combined processing and transportation of materials in industrial production lines, the winding segmented permanent magnet linear synchronous motor is preferred, and absolute position acquisition is one of the key technologies for implementation. This article focuses on a magnetoresistance absolute position detection method and error suppression strategy.

First, the arrangement form of the magnetic grid and signal-collection method of the magneto-sensitive component according to the Vernier decoding theory are presented.

Second, the error suppression in the magnetic encoder decoding system is studied deeply. Based on the error suppression strategy to improve the decoding accuracy, the RLS-DSOGI decoding technology is given. Compared with traditional decoding technology, this decoding technology can effectively suppress the amplitude, phase, and bias errors existing in the output signal of the magnetic encoder. To solve the problem of uneven distribution of data points caused by the change of motor speed, the speed weight factor was introduced to make the data points participate in the fitting calculation uniformly, which can avoid the problem of overfitting and underfitting, and improve the accuracy of parameter identification. Aiming at the problem that the dense overlapping invalid data points occupy a large amount of computing resources during the motor stop, the angle function is used to optimize the forgetting factor, which then reduces the computational pressure of the algorithm and optimizes the iterative process.

Moreover, the adaptive fitting method effectively reduces the problem of overshoot and steady-state error of the DSOGI. The proposed scheme is easy to implement and has excellent steady-state, dynamic, and anti-interference performance. It is not only suitable for winding segment-type permanent magnet linear synchronous motors, but it can also be extended to other application fields.

REFERENCES

[1] M. Mihalachi, R. Leidhold, and P. Mutschler, "Motion control for long primary linear drives used in material handling," in *Proc. 14th Int. Power Electron. Motion Control Conf. (EPE-PEMC)*, Sep. 2010, pp. T5-94–T5-101.

[2] M. Mihalachi, R. Leidhold, and P. Mutschler, "Linear drive system for combined transportation and processing of materials," in *Proc. 35th Annu. Conf. IEEE Ind. Electron.*, Nov. 2009, pp. 1185–1190.

[3] M. Mihalachi and P. Mutschler, "Capacitive sensors for position acquisition of linear drives with passive vehicles," in *Proc. 12th Int. Conf. Optim. Electr. Electron. Equip.*, May 2010, pp. 673–680.

[4] M. A. Mihalachi, "Position acquisition and control for linear direct drives with passive vehicles," Ph.D. dissertation, Vom Fachbereich Elektrotechnik und Informationstechnik der Technischen Universität Darmstadt zur Erlangung des akademischen Grades eines Doktor-Ingenieurs (Dr.-Ing.), Berlin, Germany, 2011.

[5] G. Prokofiev, V. Stakhin, V. Misevich, B. Krivtz, and M. Kosolapov, "Development of a magnetic precision position sensor based on multipolar magnetic technology," *Int. J. Appl. Eng. Res.*, vol. 13, no. 23, pp. 16656–16661, 2018.

[6] M. Benammar and A. S. P. Gonzales, "Position measurement using sinusoidal encoders and all-analog PLL converter with improved dynamic performance," *IEEE Trans. Ind. Electron.*, vol. 63, no. 4, pp. 2414–2423, Apr. 2016.

[7] R. Andraka, "A survey of CORDIC algorithms for FPGA based computers," in *Proc. ACM/SIGDA 6th Int. Symp. Field Program. Gate Arrays (FPGA)*, 1998, pp. 191–200.

[8] A. Fitzgibbon, M. Pilu, and R. B. Fisher, "Direct least square fitting of ellipses," *IEEE Trans. Pattern Anal. Mach. Intell.*, vol. 21, no. 5, pp. 476–480, May 1999.

[9] M. Karimi-Ghartemani, S. A. Khajehoddin, P. K. Jain, A. Bakhshai, and M. Mojiri, "Addressing DC component in PLL and notch filter algorithms," *IEEE Trans. Power Electron.*, vol. 27, no. 1, pp. 78–86, Jan. 2012.

[10] S. Hao, Y. Liu, and M. Hao, "Study on a novel absolute magnetic encoder," in *Proc. IEEE Int. Conf. Robot. Biomimetics*, Feb. 2009, pp. 1773–1776.

[11] F. Xiao, L. Dong, L. Li, and X. Liao, "A frequency-fixed SOGI-based PLL for single-phase grid-connected converters," *IEEE Trans. Power Electron.*, vol. 32, no. 3, pp. 1713–1719, Mar. 2017.

[12] K. Kanatani and P. Rangarajan, "Hyper least squares fitting of circles and ellipses," (in English), *Comput. Stat. Data Anal.*, vol. 55, no. 6, pp. 2197–2208, Jun. 2011.

[13] T. Mikoshiba and K. Yamasawa, "A new non-repeated code type magnetic scale using a simple absolute head," *IEEE Trans. Magn.*, vol. 32, no. 5, pp. 4938–4940, Sep. 1996.

[14] G. Prokofiev, V. Stakhin, V. Misevich, B. Krivtz, and M. Kosolapov, "Development of a specialized microcircuit for a magnetic precision position sensor based on multipolar magnetic technology," *Int. J. Appl. Eng. Res.*, vol. 14, no. 22, pp. 4143–4148, 2019.

[15] T. Shibuya, "Development of multi track magnetic ringfor high accuracy absolute angle detection," NTN, Osaka, Japan, Tech. Rev. 16, 2018.

[16] P. Freitas, J. Costa, N. Almeida, L. Melo, F. Silva, J. Bernardo, and C. Santos, "Giant magnetoresistive sensors for rotational speed control," *J. Appl. Phys.*, vol. 85, no. 8, pp. 5459–5461, 1999.

[17] Z. N. Xu and S. Y. Wang, "A highly accurate dynamic contact angle algorithm for drops on inclined surface based on ellipse-fitting," *Rev. Sci. Instrum.*, vol. 86, no. 2, Feb. 2015, Art. no. 025104.

[18] S. Golestan, M. Monfared, F. D. Freijedo, and J. M. Guerrero, "Dynamics assessment of advanced single-phase PLL structures," *IEEE Trans. Ind. Electron.*, vol. 60, no. 6, pp. 2167–2177, Jun. 2013.

[19] J. Matas, M. Castilla, J. Miret, L. G. de Vicuna, and R. Guzman, "An adaptive prefiltering method to improve the speed/accuracy tradeoff of voltage sequence detection methods under adverse grid conditions," *IEEE Trans. Ind. Electron.*, vol. 61, no. 5, pp. 2139–2151, May 2014.

[20] G. Fedele and A. Ferrise, "A frequency-locked-loop filter for biased multi-sinusoidal estimation," *IEEE Trans. Signal Process.*, vol. 62, no. 5, pp. 1125–1134, Mar. 2014.

[21] S. Golestan, M. Monfared, and F. D. Freijedo, "Design-oriented study of advanced synchronous reference frame phase-locked loops," *IEEE Trans. Power Electron.*, vol. 28, no. 2, pp. 765–778, Feb. 2013.

[22] C. Y. Wong, S. C. F. Lin, T. R. Ren, and N. M. Kwok, "A survey on ellipse detection methods," in *Proc. IEEE Int. Symp. Ind. Electron.*, May 2012, pp. 1105–1110.

[23] M. A. Alhamadi, M. Benammar, and L. Ben-Brahim, "Precise method for linearizing sine and cosine signals in resolvers and quadrature encoders applications," in *Proc. 30th Annu. Conf. Ind. Electron. Soc., (IECON)*, vol. 2, Nov. 2004, pp. 1935–1940.

[24] F. J. Rodriguez, E. Bueno, M. Aredes, L. G. B. Rolim, F. A. S. Neves, and M. C. Cavalcanti, "Discrete-time implementation of second order generalized integrators for grid converters," in *Proc. 34th Annu. Conf. IEEE Ind. Electron.*, Nov. 2008, pp. 176–181.

[25] J. Tang, A. Luo, F. Rong, Y. Wang, and Z. Huang, "Negative sequence current detection and its application," *Electr. Power Au-Tomation Equip.*, vol. 28, no. 1, pp. 23–27, 2008.
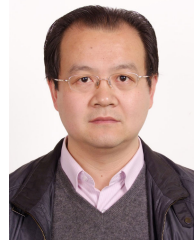
TUANSHAN ZHANG received the B.S. degree from Xi'an Polytechnic University, Xi'an, China, in 2005, and the Ph.D. degree from the Department of Mechanical Engineering, Xi'an Jiaotong University, Xi'an, specializing in electric drive transportation. He is currently an Associate Professor with the Department of Mechanical and Electrical Engineering, Xi'an Polytechnic University. He has conducted extensive research and authored more than 40 peer-reviewed articles. He holds ten patents. His research interests include design, modeling, control of battery systems, electric vehicles, renewable energy systems, and robots.

XUESONG MEI received the Ph.D. degree in mechanical engineering from Xi'an Jiaotong University, Xi'an, China, in 1991. He is currently a Full Professor with the School of Mechanical Engineering and the Director of the Shaanxi Key Laboratory of Intelligent Robots, Xi'an Jiaotong University. His research interests include intelligent manufacturing, robotics, and precision laser processing.

XIN DU was born in Shanxi, China, in 1996. He received the B.S. degree in mechanical design manufacture and automation from Shanxi Agricultural University, China, in 2019. He is currently pursuing the M.S. degree in mechanical engineering with Xi'an Polytechnic University, Xi'an, China. His research interest includes design and control of linear motors.

• • •